

# Dynamics of a vortex dipole across a magnetic phase boundary in a spinor Bose–Einstein condensate

Tomoya Kaneda<sup>1</sup> and Hiroki Saito<sup>1</sup>

<sup>1</sup>*Department of Engineering Science, University of Electro-Communications, Tokyo 182-8585, Japan*  
(Dated: March 12, 2021)

Dynamics of a vortex dipole in a spin-1 Bose–Einstein condensate in which magnetic phases are spatially distributed is investigated. When a vortex dipole travels from the ferromagnetic phase to the polar phase, or vice versa, it penetrates the phase boundary and transforms into one of the various spin vortex dipoles, such as a leapfrogging ferromagnetic-core vortex dipole and a half-quantum vortex dipole. Topological connections of spin wave functions across the phase boundary are discussed.

PACS numbers: 03.75.Mn, 03.75.Lm, 67.85.De, 67.85.Fg

## I. INTRODUCTION

A quantized vortex in a superfluid is a topological defect, and it reflects the symmetry of the macroscopic wave function. For example, a single-component Bose–Einstein condensate (BEC) is described by a complex wave function  $\psi \propto e^{i\phi}$  that has a phase degree of freedom  $\phi$ , and its symmetry group is  $U(1)$ . As a result, a vortex is characterized by an integer winding number, known as the Onsager–Feynman quantization [1, 2]. In a BEC of atoms with spin degrees of freedom, the ground-state manifold has a more complicated topology, and a variety of spin vortices exist, such as a half-quantum vortex [3] and a polar-core vortex [4]. Topological properties of spinor BECs have been studied by many researchers [5–19].

The ground-state magnetic phase of a spin-1 BEC is the ferromagnetic or polar phase depending on the interaction coefficients [20]. The symmetry group  $G_f$  of the ferromagnetic phase is  $SO(3)$  [8], i.e., there is a one-to-one correspondence between a state in the ferromagnetic phase and an element in  $G_f$ . The change in the spin state around a core of a spin vortex is therefore equivalent to a closed loop in the  $G_f$  manifold, which is classified by the fundamental group  $\pi_1(G_f) = \mathbb{Z}_2$ . For the polar phase, the symmetry group  $G_p$  is  $U(1) \times S^2/\mathbb{Z}_2$ , and its fundamental group is  $\pi_1(G_p) = \mathbb{Z}$  [12].

Let us consider a situation in which the magnetic phase containing a spin vortex changes (spatially or temporally) from the ferromagnetic to polar phases, or vice versa. Since a change in the magnetic phase is accompanied by a change in its symmetry group between  $G_f$  and  $G_p$ , the topology of a spin vortex is forced to change between elements in  $\pi_1(G_f)$  and  $\pi_1(G_p)$ . Such situations have been considered by several researchers. In Ref. [18], connections of spin-vortex lines lying on both sides of the two magnetic phases in a rotating spin-1 BEC were studied. Tracing a vortex line from one side of the magnetic phase, it undergoes various changes across the interface between the magnetic phases. In Ref. [19], structures of spin-vortex cores were studied. This problem is also regarded as the spin-vortex connection between different phases,

since the symmetry group of the spin state changes radially from infinity to the vortex core. In Ref. [21], the sudden change in the interaction parameter from polar to ferromagnetic was examined; a half-quantum vortex in the polar phase was found to magnetize breaking the rotational symmetry.

In the present paper, we investigate the dynamics of a vortex dipole (a vortex-antivortex pair) in a spin-1 BEC, where the spin-dependent interaction parameter is spatially distributed, and the ferromagnetic and polar regions are separated by a phase boundary. We create a vortex dipole on one side of the magnetic regions, and it moves toward the phase boundary. When a vortex dipole has a sufficiently large velocity, it can penetrate the phase boundary [22]. Passing through the phase boundary, the vortices experience a change in the magnetic phase, and consequently, the topological properties of the vortices are forced to change. We will show that the system exhibits a rich variety of spin dynamics that reflect the symmetry group of each magnetic phase. When a singly-quantized vortex dipole moves from the ferromagnetic to the polar phase, it transforms into a spin vortex dipole in which two ferromagnetic cores exhibit a leapfrogging behavior, or it transforms into a half-quantum vortex dipole. When a singly-quantized vortex dipole moves from the polar to the ferromagnetic phase, it transforms to a spin vortex dipole with ferromagnetic cores surrounded by half-quantum vortices.

This paper is organized as follows. Section II formulates the problem and provides a numerical method. Section III shows the dynamics of vortex dipoles traveling from ferromagnetic to polar phases, and Sec. IV shows those for traveling from polar to ferromagnetic phases. Section V presents our conclusions from this study.

## II. FORMULATION OF THE PROBLEM

We use mean-field theory to analyze a BEC of spin-1 atoms. The macroscopic wave functions  $\psi_m(\mathbf{r}, t)$  for magnetic sublevels  $m = 0, \pm 1$  obey the Gross–Pitaevskii

equation,

$$i\hbar \frac{\partial \psi_0}{\partial t} = -\frac{\hbar^2}{2M} \nabla^2 \psi_0 + g_0 \rho \psi_0 + \frac{g_1}{\sqrt{2}} (F_+ \psi_1 + F_- \psi_{-1}), \quad (1a)$$

$$i\hbar \frac{\partial \psi_{\pm 1}}{\partial t} = -\frac{\hbar^2}{2M} \nabla^2 \psi_{\pm 1} + g_0 \rho \psi_{\pm 1} + g_1 \left( \frac{1}{\sqrt{2}} F_{\mp} \psi_0 \pm F_z \psi_{\pm 1} \right), \quad (1b)$$

where  $M$  is the atomic mass and  $\rho = |\psi_1|^2 + |\psi_0|^2 + |\psi_{-1}|^2$  is the atomic density. The spin densities in Eq. (1) are defined as  $\mathbf{F} = \sum_{mm'} \psi_m^* \mathbf{f}_{mm'} \psi_{m'}$ , where  $\mathbf{f}$  is the vector of spin-1 matrices, and  $F_{\pm} = F_x \pm iF_y$ . The interaction coefficients in Eq. (1) are given by  $g_0 = 4\pi\hbar^2(a_0 + 2a_2)/(3M)$  and  $g_1 = 4\pi\hbar^2(a_2 - a_0)/(3M)$ , where  $a_0$  and  $a_2$  are the  $s$ -wave scattering lengths with colliding channels with total spin 0 and 2, respectively. For simplicity, we focus on an infinite uniform system and Eq. (1) contains no external potential terms. We assume that the quadratic Zeeman effect is negligible.

The ground-state magnetic phase depends on the sign of the interaction coefficient  $g_1$ . For  $g_1 < 0$ , the spin-dependent interaction favors the ferromagnetic ground-state. Because of the U(1) gauge and spin rotation symmetries, the ground-state manifold of the ferromagnetic state is expressed as [8]

$$\zeta = e^{i\phi} R(\alpha, \beta, \gamma) \begin{pmatrix} 1 \\ 0 \\ 0 \end{pmatrix} = e^{i(\phi-\gamma)} \begin{pmatrix} e^{-i\alpha} \cos^2 \frac{\beta}{2} \\ \sqrt{2} \sin \frac{\beta}{2} \cos \frac{\beta}{2} \\ e^{i\alpha} \sin^2 \frac{\beta}{2} \end{pmatrix}, \quad (2)$$

where  $e^{i\phi}$  and  $R(\alpha, \beta, \gamma) = e^{-if_z\alpha} e^{-if_y\beta} e^{-if_x\gamma}$  are the U(1) and SO(3) rotations, respectively. Since  $\phi$  can be absorbed into  $\gamma$  in Eq. (2), the symmetry group of the ferromagnetic state is  $G_f = \text{SO}(3)$ . For  $g_1 > 0$ , the ground state is the polar phase given by

$$\zeta = e^{i\phi} R(\alpha, \beta, \gamma) \begin{pmatrix} 0 \\ 1 \\ 0 \end{pmatrix} = e^{i\phi} \begin{pmatrix} -\frac{1}{\sqrt{2}} e^{-i\alpha} \sin \beta \\ \cos \beta \\ \frac{1}{\sqrt{2}} e^{i\alpha} \sin \beta \end{pmatrix}. \quad (3)$$

Since the state in Eq. (3) is independent of  $\gamma$  and invariant with respect to  $\alpha \rightarrow \alpha + \pi$ ,  $\beta \rightarrow \pi - \beta$ , and  $\phi \rightarrow \phi + \pi$ , the symmetry group of the polar state is  $G_p = \text{U}(1) \times S^2/\mathbb{Z}_2$ .

We consider a situation in which the interaction coefficient  $g_1$  is spatially distributed as

$$g_1(\mathbf{r}) = \begin{cases} g_f < 0 & (x < 0), \\ g_p > 0 & (x > 0), \end{cases} \quad (4)$$

where  $g_f$  and  $g_p$  are negative and positive constants, respectively. In the following, we will take  $g_f = -0.01g_0$  and  $g_p = 0.01g_0$ . Such a space-dependent interaction coefficient may be realized by, e.g., an optical Feshbach technique. For the interaction coefficient  $g_1$  in Eq. (4), the ground state is the ferromagnetic state for  $x \rightarrow -\infty$

and the polar state for  $x \rightarrow \infty$ . Their phase boundary is located at  $x \simeq 0$ , where the two phases are smoothly connected over the spin healing length. When  $\zeta|_{x \rightarrow -\infty} = (1, 0, 0)^T$ , the spin state for  $x \rightarrow \infty$  must be  $\zeta|_{x \rightarrow \infty} = (1, 0, 1)^T/\sqrt{2}$  in the ground state, where the superscript  $T$  stands for the transpose. Connection to other polar states, such as  $\zeta|_{x \rightarrow \infty} = (0, 1, 0)^T$ , does not minimize the energy.

Spin vortices in a magnetic phase with symmetry group  $G$  are classified by its fundamental group  $\pi_1(G)$ . For the ferromagnetic phase, the fundamental group of the symmetry group is  $\pi_1(G_f) = \mathbb{Z}_2$ , and there are only two topological states: no-vortex and vortex states. An expression of the vortex state far from the core located at the origin is given by  $\zeta = (e^{i\theta}, 0, 0)^T$ , where  $\theta = \arg(x + iy)$ . For the polar phase,  $\pi_1(G_p) = \mathbb{Z}$ , and corresponding vortex states are written as  $\zeta = (e^{i\theta}, 0, e^{in\theta})^T/\sqrt{2}$  with an integer  $n$ ; this is a singly-quantized vortex for  $n = 1$  and a half-quantum vortex for  $n = 0$ . The topological properties of spin vortices are thus different in the regions  $x < 0$  and  $x > 0$  for the inhomogeneous interaction coefficient  $g_1$  in Eq. (4). In the following, we study the dynamics of a vortex dipole traveling from  $x < 0$  to  $x > 0$ , or vice versa. We expect that the topology of the vortex dipole changes dynamically at the interface between the ferromagnetic and polar phases.

We numerically solve Eq. (1) using the pseudo-spectral method [23]. The initial state is the ground state for the inhomogeneous interaction coefficient  $g_1$  in Eq. (4). The ground state is numerically obtained by the imaginary-time propagation method, in which the  $i$  on the left-hand side of Eq. (1) is replaced by  $-1$ . In numerical simulations, a small numerical noise is added to the initial state to break artificial symmetry. A periodic boundary condition is imposed by the pseudo-spectral method. The size of the system is taken to be sufficiently large, and the boundary condition does not affect the dynamics of the vortices.

### III. PROPAGATION OF A VORTEX DIPOLE FROM FERROMAGNETIC TO POLAR PHASE

First we examine the dynamics of a vortex dipole traveling from the ferromagnetic phase to the polar phase. We prepare the ground state of Eq. (4), where the atomic density far from the phase boundary is  $\rho_0$ . The spin state is  $\zeta = (1, 0, 0)^T$  for  $x \ll \xi_s$ , and  $\zeta = (1, 0, 1)^T/\sqrt{2}$  for  $x \gg \xi_s$ , where  $\xi_s = \hbar/(Mg_1\rho_0)^{1/2}$  is the spin healing length. The spin healing length and the spin-wave velocity  $v_s = (g_1\rho_0/M)^{1/2}$  give the characteristic size and velocity of the spin dynamics, which define the characteristic time scale  $\tau = \xi_s/v_s$ . In the numerical simulations, a vortex dipole is created by imprinting the phase on the wave functions as

$$\psi_m(z) \rightarrow \frac{(z - z_+)(z - z_-)^*}{|(z - z_+)(z - z_-)|} \psi_m(z), \quad (5)$$

on each numerical grid, where  $z = x + iy$ , and  $z_{\pm}$  are the positions of a vortex and an antivortex. In the present initial state, we imprint the vortices at  $z_{\pm} = -5\xi_s \pm i\Delta/2$ , where  $\Delta$  is the distance between the vortex and the antivortex. The vortex dipole created on the ferromagnetic side ( $x < 0$ ) then moves in the  $+x$  direction at a velocity  $\simeq \hbar/(M\Delta)$ .

Figure 1 shows the dynamics of a vortex dipole for  $\Delta = 1.6\xi_s$ . As the vortex dipole approaches the region of  $x \simeq 0$ , the phase boundary is deformed, as shown in Fig. 1(b). Passing through the phase boundary, the vortex dipole generates a complicated spin texture, as shown in Figs. 1(c) and 1(d), and transforms into a spin vortex dipole traveling in the polar phase, as shown in Fig. 1(e). Despite the formation of the spin texture, the total density is almost homogeneous except for that of the vortex cores. Figure 1(g) shows in detail the vortex dynamics on the polar side. The cores of the vortex-antivortex pair in the  $m = \pm 1$  components are occupied by the  $m = \mp 1$  components, and the vortex dipoles in both components rotate around one another in a leapfrogging manner. We note that this dynamics is similar to the well-known leapfrogging behavior of vortices [24], but their mechanisms are quite different; this will be discussed below. As the vortex dipole travels in the polar phase, its cores gradually expand, and the total density gradually increases, as shown in Fig. 1(f). This relaxation occurs as the leapfrogging behavior causes spin wave radiation (see a movie in the Supplemental Material), dissipating the energy of the vortex dipole.

Figure 2 shows the spatiotemporal image of the magnetization density  $|\mathbf{F}|$  for the dynamics in Fig. 1. In the ferromagnetic region (red region in Fig. 2), the magnetization is  $|\mathbf{F}|/\rho_0 \simeq 1$  except for that of the vortex cores (indicated by the arrows in Fig. 2). After the penetration of the phase boundary, the vortex cores in the  $m = \pm 1$  components are occupied by the  $m = \mp 1$  components, which results in the magnetization  $F_z/\rho_0 \simeq \mp 1$  at the vortex cores. The rotation of the vortex dipoles in Fig. 1(g) is thus represented as double helices of magnetization in the spatiotemporal image in Fig. 2. The two helical structures in Fig. 2 have opposite helicities.

The results shown in Figs. 1 and 2 can be understood as follows. A singly-quantized vortex in the ferromagnetic phase is written as

$$\begin{pmatrix} e^{\pm i\theta} \\ 0 \\ 0 \end{pmatrix} f_1(r), \quad (6)$$

where the origin of the polar coordinate is taken to be the center of the vortex core, and  $f_1(r) \geq 0$  is a radial function with  $f_1(0) = 0$  and  $f_1(r)|_{r \gg \xi} = \rho_0^{1/2}$  with  $\xi = \hbar/(Mg_0\rho_0)^{1/2}$ . When the vortex in Eq. (6) enters into the polar phase, it transforms to

$$\rightarrow \frac{e^{\pm i\theta}}{\sqrt{2}} \begin{pmatrix} 1 \\ 0 \\ 1 \end{pmatrix} f_p(r) + \frac{1}{\sqrt{2}} \begin{pmatrix} 1 \\ 0 \\ -1 \end{pmatrix} f_p^{\text{core}}(r), \quad (7)$$

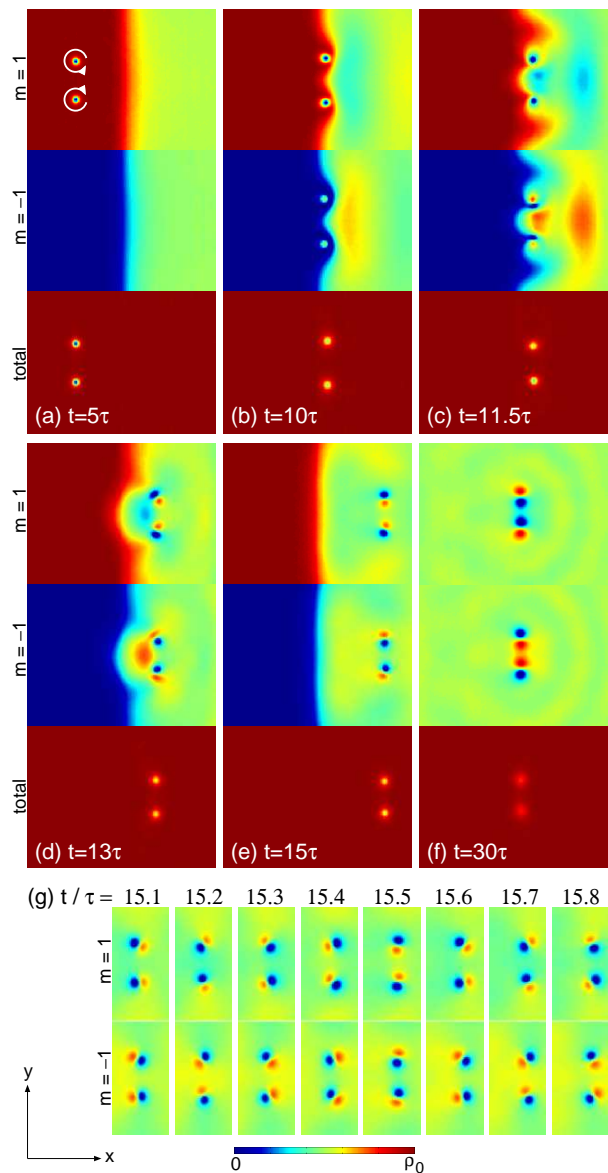


FIG. 1: (Color online) Time evolution of a vortex dipole traveling from the ferromagnetic phase to the polar phase, where the initial distance between the vortices is  $\Delta = 1.6\xi_s$ . (a)–(f) show  $|\psi_1|^2$ ,  $|\psi_{-1}|^2$ , and  $\sum_m |\psi_m|^2$ , and (g) shows  $|\psi_1|^2$  and  $|\psi_{-1}|^2$ . The density  $|\psi_0|^2$  is always negligible. The arrows in (a) indicate the directions in which the vortices circulate. The windows of each panel are (a)–(e)  $-4\xi_s < x < 4\xi_s$  and  $-3\xi_s < y < 3\xi_s$ , (f)  $10\xi_s < x < 18\xi_s$  and  $-3\xi_s < y < 3\xi_s$ , and (g)  $2\xi_s < x < 4\xi_s$  and  $-2\xi_s < y < 2\xi_s$ . Note that the scale of (f) is the same as it is for (a)–(e). See the Supplemental Material for a movie of the dynamics of  $|\psi_1|^2$ .

where the radial functions  $f_p(r), f_p^{\text{core}}(r) \geq 0$  satisfy  $f_p(0) = 0$ ,  $f_p(r)|_{r \gg \xi_s} = \rho_0^{1/2}$ , and  $f_p^{\text{core}}(r)|_{r \gg \xi_s} = 0$ , in such a way that  $f_p^{\text{core}}(r)$  occupies the core of  $f_p(r)$ . The vortex states in Eqs. (6) and (7) can be smoothly

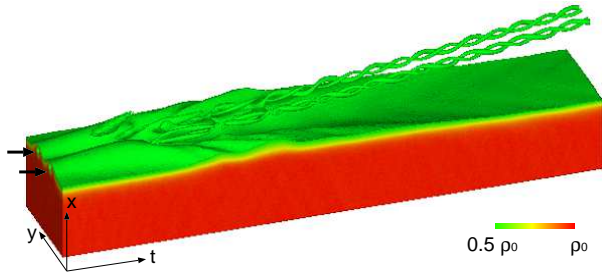


FIG. 2: (Color online) Spatiotemporal image of the magnetization density  $|\mathbf{F}|$  during  $10 < t/\tau < 16$ . The holes indicated by the arrows correspond to the vortex cores in Fig. 1(b). The parameters are the same as those in Fig. 1.

connected by an intermediate state,

$$e^{\pm i\theta} \begin{pmatrix} \cos \chi \\ 0 \\ \sin \chi \end{pmatrix} \mathcal{F}[\chi; f_1(r) \rightarrow f_p(r)] + \begin{pmatrix} -\sin \chi \\ 0 \\ \cos \chi \end{pmatrix} \mathcal{F}[\chi; 0 \rightarrow f_p^{\text{core}}(r)], \quad (8)$$

where  $\mathcal{F}$  smoothly connects the two functions as  $\chi$  changes from 0 (ferromagnetic) to  $\pi/4$  (polar). The spin state of the core (the second terms in Eqs. (7) and (8)) is taken to be such that the total density is independent of  $\theta$ . In fact, the total density is almost isotropic around the vortices, as shown in Figs. 1(a)–1(f).

We consider the time evolution of Eq. (7). Since the first and second terms in Eq. (7) may have different energies, the time evolution of Eq. (7) is written as

$$\frac{e^{\pm i\theta}}{\sqrt{2}} \begin{pmatrix} 1 \\ 0 \\ 1 \end{pmatrix} f_p(r) + \frac{1}{\sqrt{2}} \begin{pmatrix} 1 \\ 0 \\ -1 \end{pmatrix} f_p^{\text{core}}(r) e^{-i\delta\omega t}, \quad (9)$$

where  $\hbar\delta\omega$  is the energy difference between the core and the surrounding components. The magnetization of Eq. (9) is calculated to be

$$|\mathbf{F}| = |F_z| = 2f_p(r)f_p^{\text{core}}(r)|\cos(\pm\theta + \delta\omega t)|, \quad (10)$$

which has peaks at  $r \simeq \xi_s$  and  $\pm\theta + \delta\omega t = 0$  and  $\pi$ . Thus, a vortex that enters into the polar phase has two regions of nonzero magnetization around the core, and these rotate around one another at a frequency  $\delta\omega$ , resulting in the magnetization helices shown in Fig. 2. From Figs. 1(g) and 2,  $\delta\omega\tau/(2\pi)$  is found to be  $\simeq -2$ . This indicates that the energy of the core (the second term in Eq. (7)) is smaller than that of the surrounding component (the first term in Eq. (7)), since the core is not fully occupied, as shown in the total densities in Fig. 1, and hence the interaction energy is short of  $g_0\rho_0$  at the core.

The rotating vortices shown in Fig. 1(g) can also be understood to be the result of the vortex-vortex interaction in an effectively two-component BEC. In a sys-

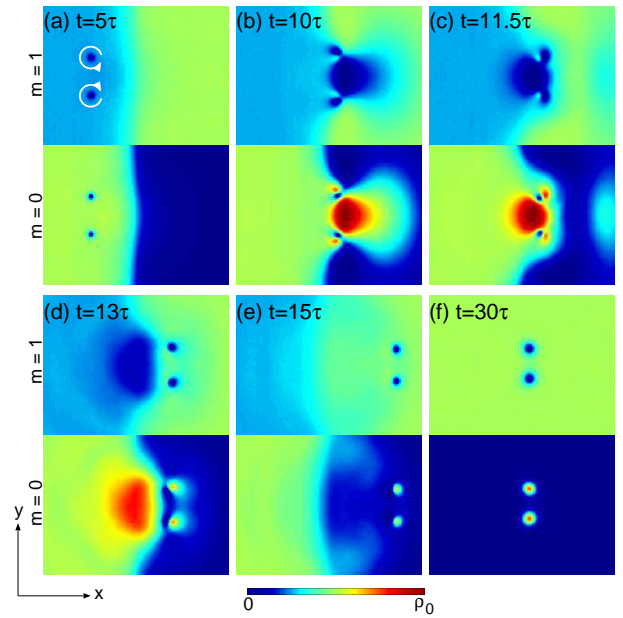


FIG. 3: (Color online) The spin states in Figs. 1(a)–1(f) are rotated by  $\pi/2$  about the  $y$  axis. The upper and lower panels show the density profiles  $|\psi_1|^2$  and  $|\psi_0|^2$ , respectively. The density  $|\psi_{-1}|^2$  is similar to  $|\psi_1|^2$ . See the Supplemental Material for a movie of the dynamics of  $|\psi_1|^2$ .

tem with inhomogeneous density, a vortex with circulation  $\kappa$  moves in the direction of  $\nabla\rho \times \kappa$ , i.e., in a direction perpendicular to the density gradient [26]. Suppose that vortices in the  $m = 1$  and  $-1$  components are located at the origin and in its vicinity, respectively. The  $m = \mp 1$  components occupy the vortex cores of  $m = \pm 1$  components, and then the  $m = -1$  density increases at the origin. Therefore, when a clockwise (counterclockwise) vortex in the  $m = -1$  component exists around the origin, it experiences a density gradient toward the origin and moves around the origin clockwise (counterclockwise). Thus, clockwise (counterclockwise) vortices in the  $m = 1$  and  $-1$  components rotate around one another clockwise (counterclockwise), as observed in Fig. 1(g). A similar behavior can also be observed in a miscible two-component BEC (data not shown).

It is interesting to see the behavior in Fig. 1 on a different spin quantization axis. Figure 3 shows the same dynamics as in Fig. 1, where  $e^{-if_y\pi/2}$  is applied to the spin state (rotation by  $\pi/2$  about the  $y$  axis). The ferromagnetic and polar states are rotated as  $e^{-if_y\pi/2}(1, 0, 0)^T = (1/2, 1/\sqrt{2}, 1/2)^T$  and  $e^{-if_y\pi/2}(1, 0, 1)^T/\sqrt{2} = (1, 0, 1)^T/\sqrt{2}$ . After the vortex dipole penetrates through the phase boundary, it becomes a vortex dipole in the  $m = \pm 1$  components, and the cores are occupied by the  $m = 0$  component, as shown in Figs. 1(e) and 1(f). Applying  $e^{-if_y\pi/2}$  to Eq. (9), we

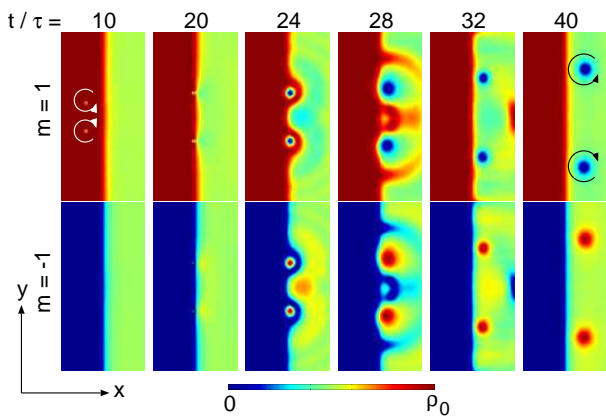


FIG. 4: (Color online) Time evolution of a vortex dipole traveling from the ferromagnetic phase to the polar phase, where the initial distance between the vortices is  $\Delta = 3.2\xi_s$ . The upper and lower panels show the density profiles  $|\psi_1|^2$  and  $|\psi_{-1}|^2$ , respectively. The density  $|\psi_0|^2$  is always negligible. The arrows indicate the directions in which the vortices circulate. The window of each panel is  $-5\xi < x < 5\xi$  and  $-10\xi < y < 10\xi$ . See the Supplemental Material for a movie of the dynamics of  $|\psi_1|^2$ .

obtain

$$\frac{e^{\pm i\theta}}{\sqrt{2}} \begin{pmatrix} 1 \\ 0 \\ 1 \end{pmatrix} f_p(r) + \begin{pmatrix} 0 \\ 1 \\ 0 \end{pmatrix} f_p^{\text{core}}(r) e^{-i\delta\omega t}. \quad (11)$$

Unlike the behavior shown in Fig. 1(g), the rotation dynamics of vortex dipoles is not observed with this spin quantization axis. The magnetization of Eq. (11) is of course the same as in Eq. (10).

Figure 4 shows the generation of a half-quantum vortex dipole, where the distance in the initial vortex dipole  $\Delta = 3.2\xi_s$  is larger than that in Figs. 1–3. As they pass through the phase boundary, the size of the vortex cores with the  $m = 1$  components significantly expand and are occupied by the  $m = -1$  components, yielding the half-quantum vortex dipole in the polar phase. The transformation from a singly-quantized vortex in the ferromagnetic phase to a half-quantum vortex in the polar phase is expressed as

$$\begin{aligned} \begin{pmatrix} e^{\pm i\theta} \\ 0 \\ 0 \end{pmatrix} f_1(r) &\rightarrow \begin{pmatrix} e^{\pm i\theta} \cos \chi \\ 0 \\ \sin \chi \end{pmatrix} \mathcal{F}[\chi; f_1(r) \rightarrow f_{\text{hqv}}(r)] \\ &+ \begin{pmatrix} 0 \\ 0 \\ 1 \end{pmatrix} \mathcal{F}[\chi; 0 \rightarrow f_{\text{hqv}}^{\text{core}}(r)] \\ &\rightarrow \frac{1}{\sqrt{2}} \begin{pmatrix} e^{\pm i\theta} \\ 0 \\ 1 \end{pmatrix} f_{\text{hqv}}(r) + \begin{pmatrix} 0 \\ 0 \\ 1 \end{pmatrix} f_{\text{hqv}}^{\text{core}}(r), \end{aligned} \quad (12)$$

where the radial functions  $f_{\text{hqv}}(r), f_{\text{hqv}}^{\text{core}}(r) \geq 0$  satisfy

$f_{\text{hqv}}(0) = 0$ ,  $f_{\text{hqv}}(r)|_{r \gg \xi_s} = \rho_0^{1/2}$ , and  $f_{\text{hqv}}^{\text{core}}(r)|_{r \gg \xi_s} = 0$ , i.e.,  $f_{\text{hqv}}^{\text{core}}(r)$  occupies the core of  $f_{\text{hqv}}(r)$ .

Thus, when a vortex dipole created in the ferromagnetic phase enters into the polar phase, it transforms into one of two kinds of spin-vortex dipoles, as shown in Figs. 1 and 4, depending on the distance  $\Delta$  in the initial vortex dipole. The leapfrogging ferromagnetic-core vortex dipoles are generated for  $\Delta \lesssim 2\xi_s$ , and the half-quantum vortex dipole is generated for  $\Delta \gtrsim 2\xi_s$ .

From a topological point of view, in general, vortex states in the ferromagnetic phase, classified by  $\pi_1(G_f) = \mathbb{Z}_2$ , and those in the polar phase, classified by  $\pi_1(G_p) = \mathbb{Z}$ , can be smoothly connected to each other [19]. In fact, spin states far from the core may be transformed from the ferromagnetic phase to the polar phase as

$$\begin{pmatrix} e^{\pm i\theta} \\ 0 \\ 0 \end{pmatrix} \rightarrow \begin{pmatrix} e^{\pm i\theta} \cos \chi \\ 0 \\ e^{in\theta} \sin \chi \end{pmatrix} \rightarrow \frac{1}{\sqrt{2}} \begin{pmatrix} e^{\pm i\theta} \\ 0 \\ e^{in\theta} \end{pmatrix}, \quad (13)$$

where  $\chi$  changes from 0 to  $\pi/4$ , and  $n$  is an integer. The dynamics shown in Figs. 1 and 4 correspond, respectively, to  $n = \pm 1$  and  $n = 0$  in Eq. (13). The transformation with other values of  $n$  are not realized in the present dynamics.

#### IV. PROPAGATION OF A VORTEX DIPOLE FROM POLAR TO FERROMAGNETIC PHASE

We next consider cases in which a vortex dipole is created in the polar phase ( $x > 0$ ) and moves toward the ferromagnetic phase ( $x < 0$ ). In Fig. 5, a vortex dipole is created at  $z_{\pm} = 5\xi_s \mp i\Delta/2$  with  $\Delta = 1.6\xi_s$ , which then moves in the  $-x$  direction. When the vortex dipole passes through the phase boundary, a complicated spin texture is formed, as shown in Figs. 5(c) and 5(d). After that, on the ferromagnetic side, a vortex dipole is transferred into the  $m = 1$  component, whose cores are occupied by the  $m = -1$  component, as shown in Fig. 5(f). Unlike the case in Fig. 1(f), the core size of the vortex dipole traveling in the ferromagnetic phase is unchanged. Figure 5(g) shows the dynamics after passing through the phase boundary, where the spin quantization axis is rotated by  $\pi/2$  about the  $y$  axis ( $e^{-if_y\pi/2}$  is applied). In this quantization axis, the vortex dipole in Fig. 5(f) behaves as leapfrogging vortex dipoles in the  $m = \pm 1$  and (12) 0 components.

The vortex transformation from that in Fig. 1(a) to

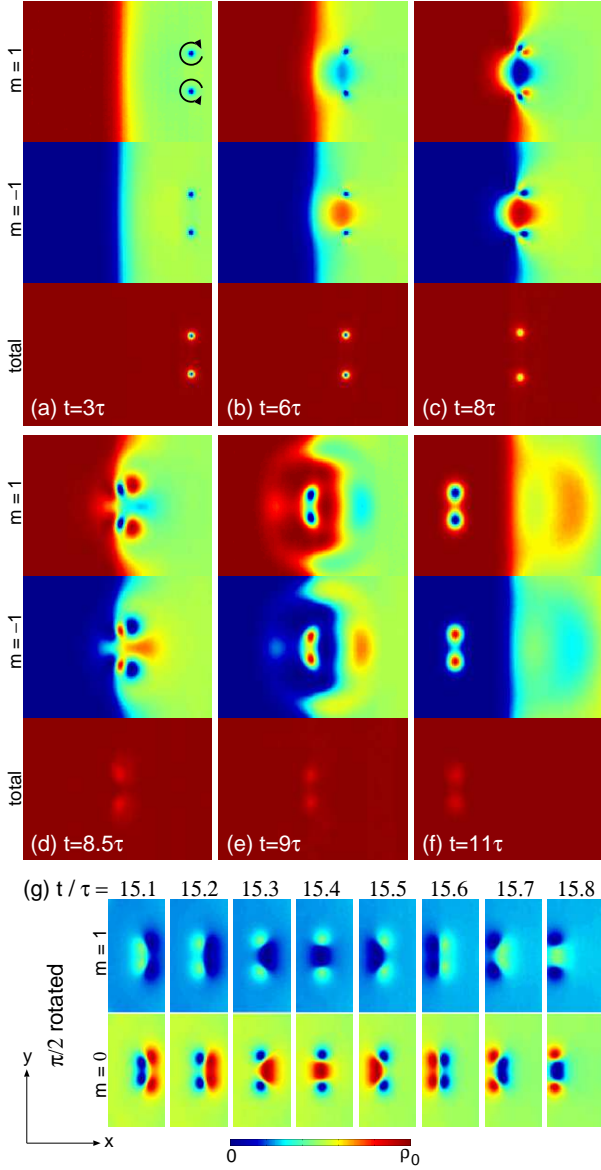


FIG. 5: (Color online) Time evolution of a vortex dipole traveling from the polar phase to the ferromagnetic phase, where the initial distance between the vortices is  $\Delta = 1.6\xi_s$ . (a)–(f) show  $|\psi_1|^2$ ,  $|\psi_{-1}|^2$ , and  $\sum_m |\psi_m|^2$ , where  $|\psi_0|^2$  is always negligible. The arrows in (a) indicate the directions in which the vortices circulate. (g) Time evolution of the density profiles  $|\psi_1|^2$  and  $|\psi_0|^2$ , where the spin quantization axis is rotated by  $\pi/2$  about the  $y$  axis. The windows of each panel are (a)–(f)  $-4\xi_s < x < 4\xi_s$  and  $-3\xi_s < y < 3\xi_s$ , and (g)  $-4.5\xi_s < x < -1.5\xi_s$  and  $-3\xi_s < y < 3\xi_s$ . See the Supplemental Material for a movie of the dynamics of  $|\psi_{-1}|^2$  in (a)–(f) and that of  $|\psi_1|^2$  in (g).

that in Fig. 1(f) is expressed as

$$\begin{aligned} \frac{e^{\pm i\theta}}{\sqrt{2}} \begin{pmatrix} 1 \\ 0 \\ 1 \end{pmatrix} f_1(r) &\rightarrow e^{\pm i\theta} \begin{pmatrix} \cos \chi \\ 0 \\ \sin \chi \end{pmatrix} \mathcal{F}[\chi; f_1(r) \rightarrow f_f(r)] \\ &+ \begin{pmatrix} -\sin \chi \\ 0 \\ \cos \chi \end{pmatrix} \mathcal{F}[\chi; 0 \rightarrow f_f^{\text{core}}(r)] \\ &\rightarrow e^{\pm i\theta} \begin{pmatrix} 1 \\ 0 \\ 0 \end{pmatrix} f_f(r) + \begin{pmatrix} 0 \\ 0 \\ 1 \end{pmatrix} f_f^{\text{core}}(r), \end{aligned} \quad (14)$$

where  $\chi$  changes from  $\pi/4$  to 0. The radial functions  $f_f(r), f_f^{\text{core}}(r) \geq 0$  satisfy  $f_f(0) = 0$ ,  $f_f(r)|_{r \gg \xi_s} = \rho_0^{1/2}$ , and  $f_f^{\text{core}}(r)|_{r \gg \xi_s} = 0$ . In the final state in Eq. (14), which corresponds to Fig. 5(f), the spin state has the form of  $\propto (e^{\pm i\theta}, 0, 1)^T$  for a radius  $r \sim \xi_s$  satisfying  $f_f(r) \simeq f_f^{\text{core}}(r)$ , which is a half-quantum vortex [19]. Thus, the vortex dipole in the ferromagnetic phase shown in Fig. 5(f) contains a half-quantum vortex dipole around the ferromagnetic cores.

Applying  $e^{-if_y\pi/2}$  to the final state in Eq. (14) and multiplying the second term by the factor  $e^{-i\delta\omega t}$ , we obtain

$$\begin{aligned} e^{\pm i\theta} \begin{pmatrix} 1/2 \\ 1/\sqrt{2} \\ 1/2 \end{pmatrix} f_f(r) + \begin{pmatrix} 1/2 \\ -1/\sqrt{2} \\ 1/2 \end{pmatrix} f_f^{\text{core}}(r) e^{-i\delta\omega t} \\ = e^{-i\delta\omega t} \begin{pmatrix} [e^{i(\pm\theta+\delta\omega t)} f_f(r) + f_f^{\text{core}}(r)]/2 \\ [e^{i(\pm\theta+\delta\omega t)} f_f(r) - f_f^{\text{core}}(r)]/\sqrt{2} \\ [e^{i(\pm\theta+\delta\omega t)} f_f(r) + f_f^{\text{core}}(r)]/2 \end{pmatrix}. \end{aligned} \quad (15)$$

Equation (15) has vortex cores at  $r \sim \xi_s$  and  $\pm\theta + \delta\omega t = \pi$  in the  $m = \pm 1$  component, and at  $\pm\theta + \delta\omega t = 0$  in the  $m = 0$  component. Thus, each component of Eq. (15) has a vortex core, and the vortices in the  $m = \pm 1$  and  $m = 0$  components rotate around one another with frequency  $\delta\omega$ , which explains the behavior in Fig. 5(g). Since the positively (negatively) charged vortices rotate around one another counterclockwise (clockwise) in Fig. 5(g),  $\delta\omega$  is found to be negative, in a manner similar to the case of Figs. 1 and 2.

We examine the dynamics of a half-quantum vortex dipole that is created on the polar side and moves toward the ferromagnetic side. In Fig. 6(a), vortices are imprinted only to the  $m = 1$  component, using Eq. (5) with  $z_{\pm} = 5\xi \mp 3.2\xi_s$ . As the half-quantum vortex dipole moves in the  $-x$  direction and approaches the phase boundary, the distance between the vortex and antivortex is reduced ( $t = 21\tau$  in Fig. 6(a)). On the ferromagnetic side, the vortex and antivortex merge into a single density hole occupied by the  $m = -1$  component, which continues to move in the  $-x$  direction ( $t = 26\tau$  in Fig. 6(a)). This is quite different from Fig. 5(f), where the vortex and antivortex survive on the ferromagnetic side. The different behaviors originate from the different energy scales of the vortices. It follows from the core

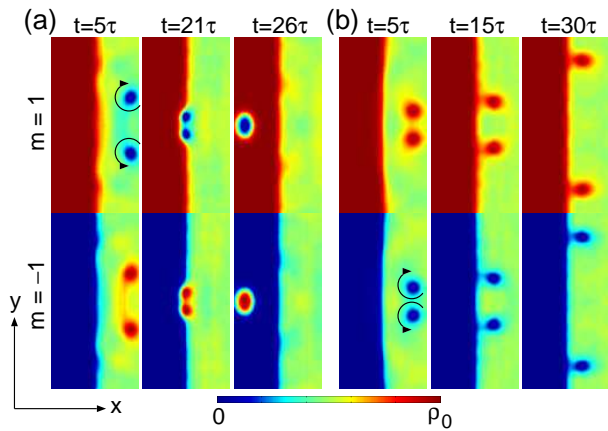


FIG. 6: (Color online) Time evolution of a system in which a half-quantum vortex dipole is imprinted to the polar side of the initial state. In (a), singly-quantized vortices are imprinted only to the  $m = 1$  wave function, and in (b), they are imprinted only to the  $m = -1$  wave function. The distances between the vortices in the initial vortex dipole are (a)  $\Delta = 6.4\xi_s$  and (b)  $\Delta = 3.2\xi_s$ . The arrows indicate the directions in which the vortices circulate. The window of each panel is  $-5\xi_s < x < 5\xi_s$  and  $-10\xi_s < y < 10\xi_s$ . See the Supplemental Material for movies of the dynamics of  $|\psi_1|^2$  in (a) and that of  $|\psi_{-1}|^2$  in (b).

sizes that the energies of the singly quantized vortices in Fig. 5(a) are larger than those of the spin vortices in Fig. 5(f), whereas the energies of the half-quantum vortices in Fig. 6(a) are smaller. Thus, the half-quantum vortex dipole cannot transform into a spin vortex dipole on the ferromagnetic side due to a lack of energy.

Figure 6(b) shows the case in which the phase is imprinted only to the  $m = -1$  initial state, using Eq. (5) with  $z_{\pm} = 5\xi \mp 1.6\xi_s$ . In this case, the penetration of a vortex dipole is topologically prohibited, since the vortices in the  $m = -1$  component cannot be smoothly connected to those in the  $m = 1$  component. The half-quantum vortex dipole therefore does not penetrate the phase boundary, but instead the vortex and antivortex disintegrate and move along the phase boundary in opposite directions, as shown in Fig. 6(b).

## V. CONCLUSIONS

We have investigated the dynamics of vortex dipoles across the boundary between the ferromagnetic and po-

lar phases in a spin-1 BEC. We numerically solved the Gross-Pitaevskii equation and found a rich variety of spin dynamics. When a singly-quantized vortex dipole is created on the ferromagnetic side and propagated toward the polar side, it transforms into one of two kinds of spin-vortex dipoles, depending on its velocity. For a large velocity, ferromagnetic-core vortex dipoles are created in the  $m = 1$  and  $-1$  components, which exhibit the leapfrogging dynamics, as shown in Figs. 1 and 2. For a small velocity, a half-quantum vortex dipole is generated, as shown in Fig. 4. When a singly-quantized vortex dipole created on the polar side moves into the ferromagnetic side, it transforms into a vortex dipole whose ferromagnetic cores are surrounded by half-quantum vortices, as shown in Figs. 5(a)–5(f). This state also exhibits the leapfrogging behavior on a different quantization axis, as shown in Fig. 5(g). When a half-quantum vortex dipole is created on the polar side and propagated to the ferromagnetic side, it coalesces into a low energy droplet or is turned away at the phase boundary, as shown in Fig. 6.

We have considered an ideal system that is infinite and homogeneous. In a realistic experimental system confined in a trapping potential, the system size must be much larger than a vortex dipole and its trajectory. An elongated oblate BEC, as used in the Berkeley experiment [4], would be suitable. An initial vortex dipole can be created by an external laser beam shifting in a BEC [25, 26]. A half-quantum vortex-dipole, as shown in Fig. 6, may be created by an  $m$ -dependent external potential [27, 28].

Our study presents an example of the dynamical transformation of topological defects, in which topological structures are dynamically changed. It will also be interesting to consider collisions of topological defects. During collisions, topological structures may be dynamically changed, and different topological structures may be scattered after the collisions, which might be relevant to the collisions of elementary particles.

## Acknowledgments

This work was supported by JSPS KAKENHI Grant Number 26400414 and by KAKENHI (No. 25103007, “Fluctuation & Structure”) from MEXT, Japan.

- 
- [1] L. Onsager, Nuovo Cimento Suppl. **6**, 249 (1949).  
 [2] R. P. Feynman, Prog. Low Temp. Phys. **1**, 17 (1955).  
 [3] U. Leonhardt and G. E. Volovik, JETP Letters **72**, 46 (2000).  
 [4] L. E. Sadler, J. M. Higbie, S. R. Leslie, M. Vengalattore,

- and D. M. Stamper-Kurn, Nature (London) **443**, 312 (2006).  
 [5] J. Y. Choi, W. J. Kwon, and Y. I. Shin, Phys. Rev. Lett. **108**, 035301 (2012).  
 [6] M. W. Ray, E. Ruokokoski, S. Kandel, M. Möttönen, and

- D. S. Hall, *Nature (London)* **505**, 657 (2014).
- [7] T. Ohmi and K. Machida, *J. Phys. Soc. Jpn.* **67**, 1822 (1998).
- [8] T. -L. Ho, *Phys. Rev. Lett.* **81**, 742 (1998).
- [9] U. A. Khawaja and H. T. C. Stoof, *Nature (London)* **411**, 918 (2001); *Phys. Rev. A* **64**, 043612 (2001).
- [10] C. M. Savage and J. Ruostekoski, *Phys. Rev. A* **68**, 043604 (2003).
- [11] J. Ruostekoski and J. R. Anglin, *Phys. Rev. Lett.* **91**, 190402 (2003).
- [12] H. Mäkelä, Y. Zhang, and K. -A. Suominen, *J. Phys. A: Math. Gen.* **36**, 8555 (2003).
- [13] G. W. Semenoff and F. Zhou, *Phys. Rev. Lett.* **98**, 100401 (2007).
- [14] R. Barnett, A. Turner, and E. Demler, *Phys. Rev. A* **76**, 013605 (2007).
- [15] Y. Kawaguchi, M. Nitta, and M. Ueda, *Phys. Rev. Lett.* **100**, 180403 (2008).
- [16] M. Kobayashi, Y. Kawaguchi, M. Nitta, and M. Ueda, *Phys. Rev. Lett.* **103**, 115301 (2009).
- [17] V. Pietilä and M. Möttönen, *Phys. Rev. Lett.* **103**, 030401 (2009).
- [18] M. O. Borgh and J. Ruostekoski, *Phys. Rev. Lett.* **109**, 015302 (2012); *Phys. Rev. A* **87**, 033617 (2013).
- [19] S. Kobayashi, Y. Kawaguchi, M. Nitta, and M. Ueda, *Phys. Rev. A* **86**, 023612 (2012).
- [20] J. Stenger, S. Inouye, D. M. Stamper-Kurn, H. -J. Miesner, A. P. Chikkatur, and W. Ketterle, *Nature (London)* **396**, 345 (1998).
- [21] S. Hoshi and H. Saito, *Phys. Rev. A* **78**, 053618 (2008).
- [22] T. Aioi, T. Kadokura, and H. Saito, *Phys. Rev. A* **85**, 023618 (2012).
- [23] W. H. Press, S. A. Teukolsky, W. T. Vetterling, B. P. Flannery, *Numerical Recipes*, 3rd ed, Sec. 20.7 (Cambridge Univ. Press, Cambridge, 2007).
- [24] H. von Helmholtz, *Crelle's J.* **55**, 25 (1858) [*Philos. Mag. Ser. 4* **33**, 485 (1867)].
- [25] T. W. Neely, E. C. Samson, A. S. Bradley, M. J. Davis, and B. P. Anderson, *Phys. Rev. Lett.* **104**, 160401 (2010).
- [26] T. Aioi, T. Kadokura, T. Kishimoto, and H. Saito, *Phys. Rev. X* **1**, 021003 (2011).
- [27] A. -C. Ji, W. M. Liu, J. L. Song, and F. Zhou, *Phys. Rev. Lett.* **101**, 010402 (2008).
- [28] H. Chiba and H. Saito, *Phys. Rev. A* **78**, 043602 (2008).